# Formation of Self-Organized $TiO_2$ Nanotube Arrays and Its Photoelectrochemical Response

**Hawraa Sabah Hreo[a], Araa Mebdir Holi[a,*], Asmaa Kadim Ayal[b]**

[a] Department of Physics, College of Education, University of Al-Qadisiyah, Al-Diwaniyah, Al-Qadisiyah 58002, Iraq

[b] Department of Chemistry, College of Science for Women, University of Baghdad, Baghdad, Iraq

E-mail: araa.holi@qu.edu.iq



**Abstract**

In this study, TiO2 nanotube arrays (TNTAs) are produced using an efficient, low-cost, and ecofriendly environmental anodization process in an electrolyte containing Glycerin. The TNTAs were annealed for 2 hours at 500 °C. X-ray diffraction (XRD), scanning electron microscopy (FE-SEM), UV-Vis diffuse reflectance spectroscopy (DRS), photoluminescence (PL), and photoelectrochemical properties (PEC) were used to analyze the sample. According to the obtained findings, the photoelectrochemical response of the TiO2 film was accomplished with a current density (Jph) of 0.196 mAcm-2 and photoconversion efficiency of 0.14%.

**Keywords:** Anodization; Glycerin; Titanium dioxide; Nanotubes arrays.

## 1. Introduction

Titanium dioxide ($TiO_2$) has gotten a lot of interest because of its unique features [1]. $TiO_2$ is a one-of-a-kind material because of its chemical, electrical, morphological, excellent optical properties, and high surface-to-volume ratio. $TiO_2$ is a one-of-a-kind substance. $TiO_2$ in the form of high-quality nanotube bundled structures has the potential to improve a broad range of applications' performance. It has a wide range of applications, namely solar cells[2][3], photocatalysis [4][5][6], as well as gas sensors. $TiO_2$ (TNT) is an especially effective photocatalyst for hydrogen generation [7][8], photoelectrochemical cell since 1972 [9], and oxidation by electrocatalysis [10][11]. $TiO_2$'s application range continues to grow, including biosensors[12][13]. In recent years, the fabrication of titania nanostructured has accelerated significantly[14]. Titania can be formed using various techniques, including sol-gel [15], electrodeposition [16], hydrothermal method [17], and anodization procedure [18] [19]. The anodizing method is the most widely used because it is considered extremely beneficial, productive, inexpensive and simple to perform, and it does not require high temperatures. It is prepared at room temperature [19-21]. Improved TNT morphology can be achieved by adjusting the anodization time, electrolyte composition, and applied voltage [22]. The electrolyte composition [75 ml Glycerin + 25 ml water + 0.5g $NH_4F$] was used as an electrolyte composition in this investigation to improve the anodic growth of self-organized $TiO_2$ nanotubes.

## 2. Experimental

### 2. 1. Fabrication $Tio_2$ Nanotubes

Cutting a sheet of titanium foil into (2.5x1) $cm^2$ is the first step. After fifteen minutes of treatment with ultrasonic in acetone, isopropanol, and deionized water (DI), the pieces were chemically reduced, respectively. Following that, they were immersed for 10 minutes in a solution of 6 M $HNO_3$ to smooth out the surface. The anodizing procedure was accomplished by a consisting cell of two electrodes configuration. The working electrode was titanium foil, with high-density graphite serving as the counter electrode. A constant two-centimeter distance was maintained throughout the experiment. After an hour of anodization at 30V, a D.C power supply (MP6010D) was used for anodizing the titanium, as shown in Figure 1. Then, the anodization process was prepared using an electrolytic composition [75 ml Glycerin + 25 ml water + 0.5g $NH_4F$]. Following the preparation of the sample, it was washed with deionized water. The film was annealed in a thermo-oven at 500 degrees Celsius for two hours. During the electrochemical anodization of titanium in a fluoride-based electrolyte, three sequential processes occurred; see Figure 1A. In the beginning, Ti is oxidized to $TiO_2$, thin oxide layer forms on the titanium surface, Figure 1B. As a result of this reaction, fluoride anions ($F^-$) are deposited on the Ti surface, resulting in a porous thin film, Figure 1C.

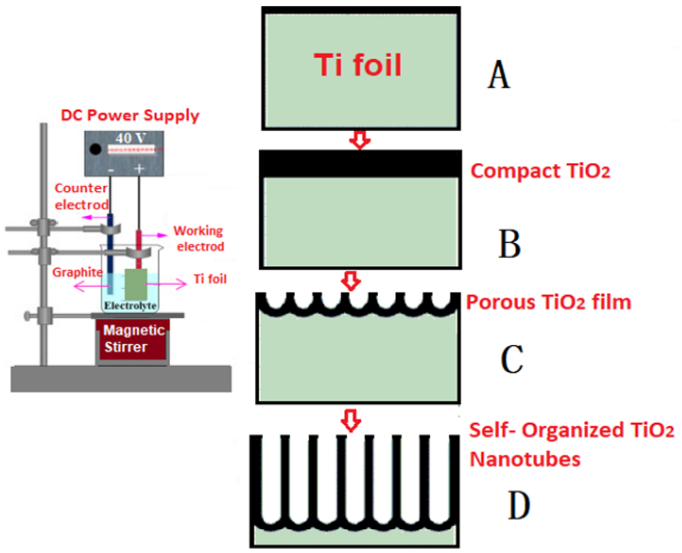


Fig 1. Schematic diagram of anodization method setup and formation steps of $TiO_2$ NTs; A: Ti foil (titanium metal); B: compact $TiO_2$ ($TiO_2$ thin film); C: porous $TiO_2$ film; D: $TiO_2$ NTs.

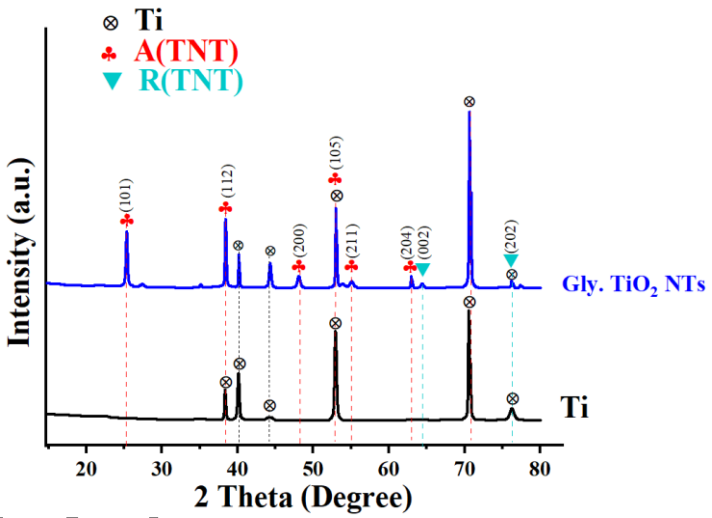


Fig 2. The XRD patterns for Ti foil and $TiO_2$ nanotubes.

Lastly, the surface-bound soluble titanium fluoride complex $[(TiF_6)_2]$ dissipated slowly, creating porous $TiO_2$ NT structures, Figure 1D.

### 2.2 Characterization

Shimadzu XRD-6000 Diffractometer, which has a scanning range of 20°–80°, was used to analyze the XRD patterns of the photoanode. The photo anode's morphology was analyzed utilizing a scanning electron microscope for field emission (Nano SEM 450) coupled with energy-dispersive spectroscopy (EDX). The PL emission spectra were obtained using a Perkin–Elmer LS-55 spectrophotometer. Spectra of diffuse reflectance in the UV-visible region (DRS) between 200 and 800 nm were recorded using a double beam solid-state Shimadzu TM model DUV 3700 spectrophotometer. The Kubelka-Munk theory and Tauc plot were used to analyze the bandgap energy of sample. To evaluate the PEC performance of $TiO_2$, a three-electrode electrochemical cell was constructed. There were three types of electrodes used in this experiment: working electrodes made of $TiO_2$ NTs and $Bi_2S_3$/TNTs samples, a platinum (Pt) counter electrode and an (Ag/AgCl) reference electrode. The electrolyte cell was obtained using mixed $Na_2SO_3$ (0.1 M) and $Na_2S$ (0.1 M). Measurement of photocurrent density (Gamry Instrument framework interface with 1000 E Potentiostat/Galvanostat/ZRA) was carried out using the LSV technique. In the presence Fully Reflective Solar Simulator (SS1.6kW), the effect of the potential between (-1.2 and +1.2 V) versus Ag/AgCl at a scan rate of 20 $mVs^{-1}$ was found. Newport's xenon lamp simulated solar irradiation in the atmosphere and on the ground. By ASTM G173-03(2012), the lamp's output intensity matched the solar irradiance spectrum. The xenon lamp's light was focused on a quartz reaction cell (15 cm apart) with a 1 cm square working electrode area. During regular intervals, the manual chopping provided the light source, which had an irradiance of 100 $mW/cm^2$, which was equivalent to one sun lighting. The proposed $TiO_2$ NTs photoconversion efficiency (η%) was evaluated using the expression [23].

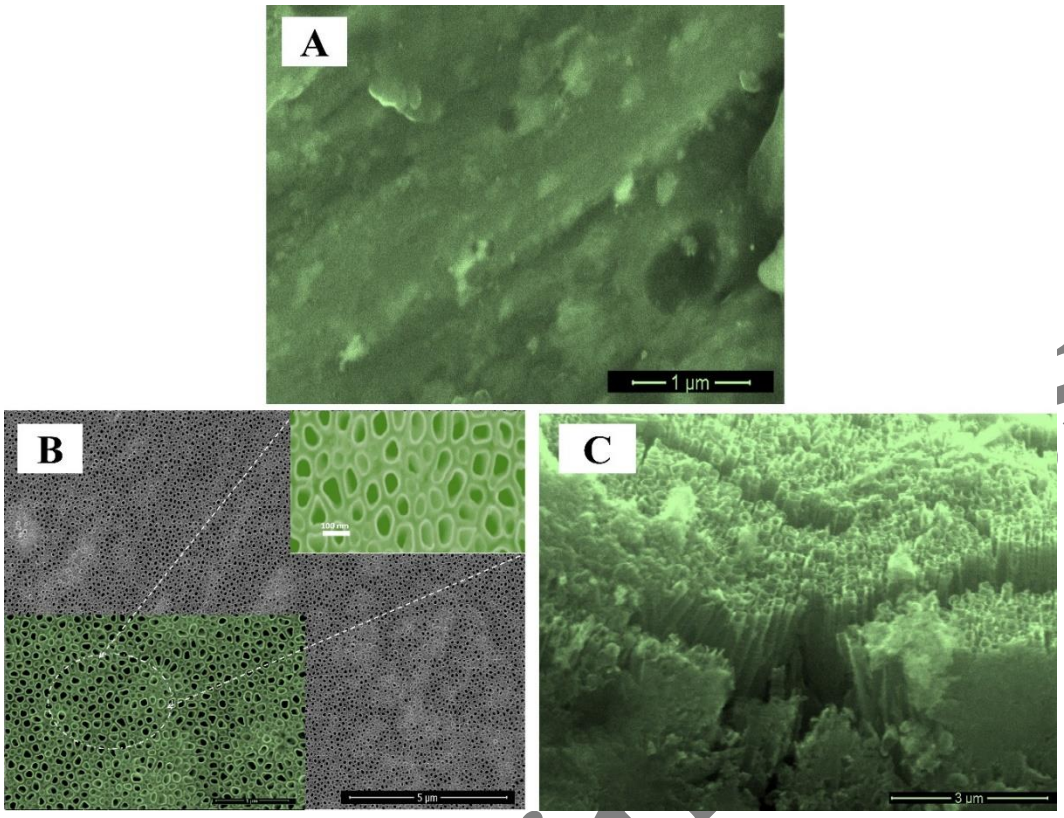


Fig. 3 FE-SEM images of (A) The top-view and (B) The cross-sectional view of the $TiO_2$ nanotubes.

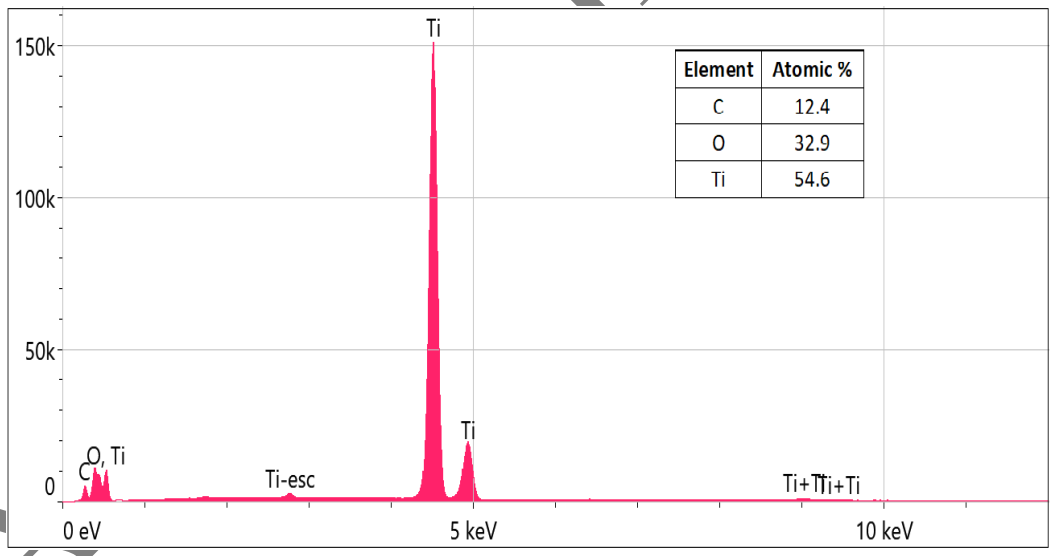


Fig. 4. EDX spectra of $TiO_2$ NTs.

## 3. Results and Discussion

### 3. 1. X-Ray Diffraction

Figure 2 shows the X-ray diffraction patterns of Ti and $TiO_2$ NTs from 10° to 80° (2theta). The first pattern shows diffraction peaks corresponding to metallic Ti used as an anodizing substrate. After the Ti foil was anodized, all new peaks were matched to the standard tetragonal $TiO_2$ NTs rutile and anatase phases (JCPDS card number 021-1272) and (JCPDS card 021-1276). Crystallinity is sufficient to see the highest peak at 25.30° of an anatase phase in the lattice plane (101). Debye-formula Scherers can be used to figure out the prepared sample [24]. $D=0.9\lambda/\beta\cos\theta$. 32.8 nm was the crystallite size of $TiO_2$ NTs and this result agree with the researcher [25].

### 3. 2. Morphological and EDX Analysis

Figure 3 depicts scanning electron microscopy images of plain Ti foil, and $TiO_2$ nanotubes synthesized by anodization treatment at 30V for 1 hour in a glycerin electrolyte. Results show that nanotube walls were formed in regular shapes with wide pores, as shown in Figure 3B.

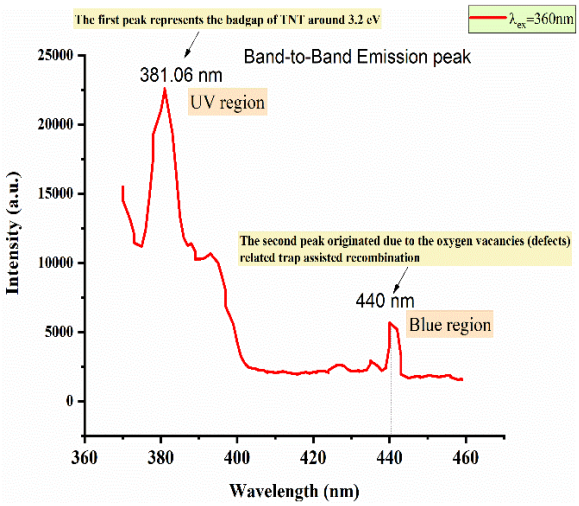


Fig 5. The PL spectra of $TiO_2$ NTs.

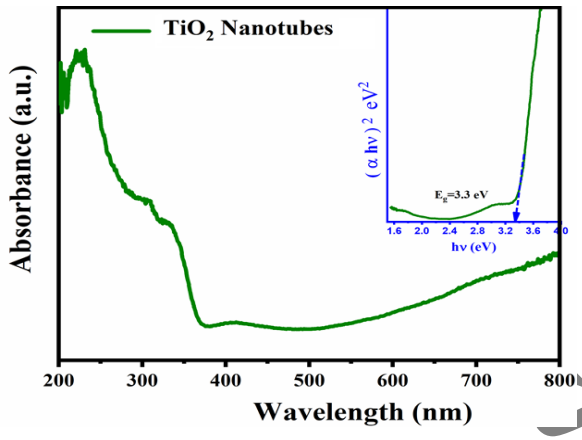


Fig 6. UV-vis diffuse reflectance spectra (DRS) for $TiO_2$ NTs.

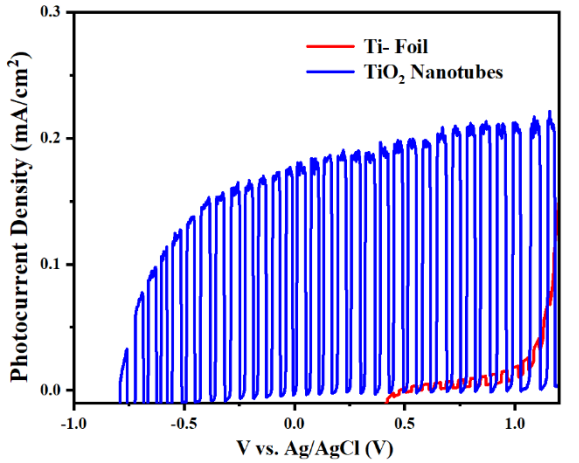


Fig 7. Linear sweep voltammograms for plain Ti foil and $TiO_2$ NTs obtained at a scan rate of 20 $mVs^{-1}$ at applied potentials ranging from -1.2 V to +1.2 V using a 100 $mWcm^2$ illumination source in 0.1 M $Na_2S$ and $Na_2SO_3$ electrolyte.

Table 1. shows the C.B. and V.B. values of $TiO_2$ NTs.

| Photoanode construction | $E_g$ (eV) | vs. NHE | | vs. Vacuum | |
|---|---|---|---|---|---|
| | | C.B (eV) | V.B (eV) | C.B (eV) | V.B (eV) |
| $TiO_2$ NTs | 3.3 | -0.33 | 2.970 | -4.175 | -7.475 |

The tube diameter of the sample was measured using image analysis software (Digimizer), and the average diameter of $TiO_2$ NTs was found to be 100±25 nm. As depicted in Figure 3C, cross-sectional image of this sample reveal a thick and aligned tube with a length of approximately 5± 300 µm, and these findings are consistent with those of the researcher [26].

The elemental composition of the sensitized $TiO_2$ nanotubes was determined using EDX spectroscopy. Figure 4 shows the EDX spectrum of the $TiO_2$ NTs sample, which confirms that it contains the components (C, O, and Ti). A small carbon peak at 0.27 keV is due to the carbon coating of the sample.

### 3. 3. Photoluminescence (PL) Test

In Figure 5, the P.L. spectrum exhibits the strongest emission peak centered at 381 nm under the excitation wavelength of 360 nm. The oxygen vacancies, surface faults, and self-trapped excitons dominate the P.L. spectrum of $TiO_2$ anatase [25]. The band–band transition in $TiO_2$ produces a peak at around 381 nm [26-27]. At approximately 440 nanometers, there is an obvious photoluminescence peak. This is most likely due to the oxygen vacancies (defects) related trap assisted recombination.

### 3. 4 UV-Vs spectral analysis

The UV-Vis diffuse reflectance spectra (DRS) of $TiO_2$ nanotubes are shown in Figure 6. It illustrates the optical absorption edge of $TiO_2$ nanotubes, which is detected at approximately 400 nanometers, and indicates that the bandgap for $TiO_2$ NTs is 3.3 eV. The results show a majority of the UV light absorption by $TiO_2$ nanotubes occurs below 400 nm. This is because of the relative wide the bandgap of $TiO_2$ (3.3 eV), and these results are similar to what the researcher came up with [27].

### 3. 5 PEC performance

The photoelectrochemical measurements of the plain Ti and $TiO_2$ NTs in the electrolyte as shown in Figure 7. The photocurrent responses of the Ti foil and $TiO_2$ NTs are around 7.4 µA/$cm^2$ and 0.196 mA/$cm^2$, respectively. To study the photoelectrochemical performance of $TiO_2$ NTs, it is important to understand their band edge potentials, the migration manner of photogenerated electrons and holes is strongly influenced by the band edge potential. This empirical equation can be used to predict the $TiO_2$ NT's valence and conduction bands [28].

$$E_{C.B} = \chi - 0.5\, E_g + E_o \quad (1)$$

$$E_{V.B} = E_{C.B} + E_g \quad (2)$$

Here, the valence and conduction band edge potentials are $E_{V.B.}$ and $E_{C.B.}$, and the value of $\chi$ indicates the constituent atoms' electronegativity. ($E_o$) is an electron's energy (- 4.5 eV), and Eg denotes the semiconductor's bandgap energy. Table 1 shows the results of the above equations, with the $\chi$ values of $TiO_2$ being 5.82 eV,[29].

## 4. Conclusion

In conclusion, the use of glycerine as a solution composition in the construction of titanium dioxide nanotube arrays $TiO_2$ NTs has been investigated. It was created throughout a simple anodization method in

electrolytes containing small amounts of fluoric ions. The development of nanotube arrays with a photoelectrochemical response (0.196 mA/cm$^2$) came from the application of a $TiO_2$ anodic layer over a vast and continuous area on the primary Ti substrate. High-quality nanotube bundled structures made of $TiO_2$ have the potential to increase the performance of a number of applications, including photoelectrochemical cells.

## 5. References


1. S. H. Kang, W. Lee, Y.-C. Nah, K.-S. Lee, and H. S. Kim, "Synthesis of nanobranched TiO2 nanotubes and their application to dye-sensitized solar cells," Curr. Appl. Phys., vol. 13, no. 1, pp. 252–255, 2013.
2. O. K. Varghese, M. Paulose, and C. A. Grimes, "Long vertically aligned titania nanotubes on transparent conducting oxide for highly efficient solar cells," Nat. Nanotechnol., vol. 4, no. 9, pp. 592–597, 2009.
3. J. Yuan and S. Tsujikawa, "Characterization of sol-gel-derived TiO2 coatings and their photoeffects on copper substrates," J. Electrochem. Soc., vol. 142, no. 10, p. 3444, 1995.
4. Y. Guo, J. Hu, H. Liang, L. Wan, and C. Bai, "TiO2-Based Composite Nanotube Arrays Prepared via Layer-by-Layer Assembly," Adv. Funct. Mater., vol. 15, no. 2, pp. 196–202, 2005.
5. G. K. Mor, K. Shankar, M. Paulose, O. K. Varghese, and C. A. Grimes, "Use of highly-ordered TiO2 nanotube arrays in dye-sensitized solar cells," Nano Lett., vol. 6, no. 2, pp. 215–218, 2006.
6. A. Z. Fatichi et al., "Crystalline phase of TiO2 nanotube arrays on Ti–35Nb–4Zr alloy: Surface roughness, electrochemical behavior and cellular response," Ceram. Int., vol. 48, no. 4, pp. 5154–5161, 2022.
7. Y. Li, Y. Xiang, S. Peng, X. Wang, and L. Zhou, "Modification of Zr-doped titania nanotube arrays by urea pyrolysis for enhanced visible-light photoelectrochemical H2 generation," Electrochim. Acta, vol. 87, pp. 794–800, 2013.
8. W. Krengvirat, S. Sreekantan, A.-F. M. Noor, G. Kawamura, H. Muto, and A. Matsuda, "Single-step growth of carbon and potassium-embedded TiO2 nanotube arrays for efficient photoelectrochemical hydrogen generation," Electrochim. Acta, vol. 89, pp. 585–593, 2013.
9. C. W. Lai and S. Sreekantan, "Incorporation of WO3 species into TiO2 nanotubes via wet impregnation and their water-splitting performance," Electrochim. Acta, vol. 87, pp. 294–302, 2013.
10. H. He et al., "PtNi alloy nanoparticles supported on carbon-doped TiO2 nanotube arrays for photo-assisted methanol oxidation," Electrochim. Acta, vol. 88, pp. 782–789, 2013.
11. Y.-Y. Song, Z.-D. Gao, and P. Schmuki, "Highly uniform Pt nanoparticle decoration on TiO2 nanotube arrays: a refreshable platform for methanol electrooxidation," Electrochem. commun., vol. 13, no. 3, pp. 290–293, 2011.
12. A. K. M. Kafi, G. Wu, P. Benvenuto, and A. Chen, "Highly sensitive amperometric H2O2 biosensor based on hemoglobin modified TiO2 nanotubes," J. Electroanal. Chem., vol. 662, no. 1, pp. 64–69, 2011.
13. S. Yu et al., "Ni nanoparticles decorated titania nanotube arrays as efficient nonenzymatic glucose sensor," Electrochim. Acta, vol. 76, pp. 512–517, 2012.
14. Y. Lai et al., "Bioinspired patterning with extreme wettability contrast on TiO2 nanotube array surface: a versatile platform for biomedical applications," Small, vol. 9, no. 17, pp. 2945–2953, 2013.
15. M. Zhang, Y. Bando, and K. Wada, "Sol-gel template preparation of TiO2 nanotubes and nanorods," J. Mater. Sci. Lett., vol. 20, no. 2, pp. 167–170, 2001.
16. Q. Y. Zeng, M. Xi, W. Xu, and X. J. Li, "Preparation of titanium dioxide nanotube arrays on titanium mesh by anodization in (NH4)2SO4/NH4F electrolyte," Mater. Corros., vol. 64, no. 11, pp. 1001–1006, 2013, doi: 10.1002/maco.201106481.
17. H.-H. Wang et al., "Preparation of nanoporous TiO2 electrodes for dye-sensitized solar cells," J. Nanomater., vol. 2011, 2011.
18. L. Yao, J. Chen, Z. Wang, and T.-K. Sham, "TiO2 Nanotubes: Morphology, Size, Crystallinity, and Phase-Dependent Properties from Synchrotron-Spectroscopy Studies," J. Phys. Chem. C, vol. 126, no. 6, pp. 3265–3275, 2022.
19. J. Dong et al., "Defective black TiO2 synthesized via anodization for visible-light photocatalysis," ACS Appl. Mater. Interfaces, vol. 6, no. 3, pp. 1385–1388, 2014.
20. R. Hahn, J. M. Macak, and P. Schmuki, "Rapid anodic growth of TiO2 and WO3 nanotubes in fluoride free electrolytes," Electrochem. commun., vol. 9, no. 5, pp. 947–952, 2007.
21. S. Sreekantan, K. A. Saharudin, and L. C. Wei, "Formation of TiO2 nanotubes via anodization and potential applications for photocatalysts, biomedical materials, and photoelectrochemical cell," IOP Conf. Ser. Mater. Sci. Eng., vol. 21, no. 1, 2011, doi: 10.1088/1757-899X/21/1/012002.
22. Y. Lai et al., "Y. Lai et al., 'Bioinspired patterning with extreme wettability contrast on TiO2 nanotube array surface: a versatile platform for biomedical applications,' Small, vol. 9, no. 17, pp. 2945–2953, 2013.," Small, vol. 9, no. 17, pp. 2945–2953, 2013.
23. X. Dong, W. Huang, and P. Chen, "In situ synthesis of reduced graphene oxide and gold nanocomposites for nanoelectronics and biosensing," Nanoscale Res Lett, vol. 6, no. 1, pp. 1–6, 2011.
24. D. Louër and N. Audebrand, "Profile fitting and diffraction line broadening analysis," Adv. x-ray Anal., vol. 41, pp. 556–565, 1999.
25. J. Georgieva et al., "A simple preparation method and characterization of B and N co-doped TiO2 nanotube arrays with enhanced photoelectrochemical performance," Appl. Surf. Sci., vol. 413, pp. 284–291, 2017.
26. J. Gong, W. Pu, C. Yang, and J. Zhang, "Novel one-step preparation of tungsten loaded TiO2 nanotube arrays with enhanced photoelectrocatalytic activity for pollutant degradation and hydrogen production," Catal. Commun., vol. 36, pp. 89–93, 2013.
27. A. E. R. Mohamed and S. Rohani, "Modified TiO2 nanotube arrays (TNTAs): progressive strategies towards visible light responsive photoanode, a review," Energy Environ. Sci., vol. 4, no. 4, pp. 1065–1086, 2011.
28. A. Helal, F. A. Harraz, A. A. Ismail, T. M. Sami, and I. A. Ibrahim, "Hydrothermal synthesis of novel heterostructured Fe2O3/Bi2S3 nanorods with enhanced photocatalytic activity under visible light," Appl. Catal. B Environ., vol. 213, pp. 18–27, 2017.
29. A. K. Ayal et al., "Electrochemical deposition of CdSe-sensitized TiO2 nanotube arrays with enha," J. Mater. Sci. Mater. Electron., vol. 27, no. 5, pp. 5204–5210, 2016, doi: 10.1007/s10854-016-4414-8.